

# Three dimensional characteristics of biopores and non-biopores in the subsoil respond differently to land use and fertilization

Zhongbin Zhang · Kailou Liu · Hu Zhou · Henry Lin · Daming Li · Xinhua Peng

Received: 31 January 2018 / Accepted: 17 May 2018 / Published online: 28 May 2018  
© Springer International Publishing AG, part of Springer Nature 2018

## Abstract

**Background and aims** Soil macropores consist of biopores and non-biopores, which are different in morphological features and ecological functions. We aimed to separate biopores and non-biopores and investigate the response of their three-dimensional (3D) characteristics to land use and fertilization.

**Methods** Intact soil cores sampled from the subsoil (20–30 cm) under a combination of two land uses, paddy and upland fields, and three fertilization treatments, no fertilizer (Control), chemical fertilizer (NPK), and chemical fertilizer plus organic manure (NPKM), were scanned with X-ray computed tomography (CT). A methodology was proposed to separate biopores and non-biopores and the 3D characteristics of the pores were quantified.

**Results** Based on the proposed methodology, soil biopores were well isolated from non-biopores. The volume of the biopores contributed 30.1–58.0% and 66.3–74.1% of the volume of the total macropores in the upland

and paddy subsoils, respectively. The biopores in the paddy subsoil had a lower mean pore volume (MPV) and mean branch number (MBN), but a larger branch angle than those of the biopores found in the upland subsoil. The porosity, MPV, surface area (SA) and connectivity of non-biopores were significantly higher in the upland subsoil than those in the paddy subsoil. The NPKM treatment significantly increased the volume of the large-sized biopores in the upland subsoil and the tortuosity of the biopores in the paddy subsoil, whereas the fertilization effect on non-biopores was minor.

**Conclusions** Our results demonstrate that subsoil biopores and non-biopores can be effectively distinguished according to the proposed methodology and that their 3D characteristics respond differently to land use and fertilization.

**Keywords** Soil structure; biopores · Computed tomography · Land use · Fertilization

---

Responsible Editor: W Richard Whalley.

Z. Zhang · H. Zhou · X. Peng (✉)  
State Key Laboratory of Soil and Sustainable Agriculture, Institute of Soil Science, CAS, Nanjing 210008, China  
e-mail: xhpeng@issas.ac.cn

K. Liu · D. Li  
National Engineering and Technology Research Center for Red Soil Improvement, Jiangxi Institute of Red Soil, Nanchang 331717, China

H. Lin  
Department of Ecosystem Sciences and Management, Pennsylvania State University, University Park, PA 16802, USA

## Introduction

Soil pore systems have essential soil functions in ecosystems, such as conducting water or gas, providing space for root growth, and sheltering soil fauna (Athmann et al. 2013; Katuwal et al. 2015; Lamandé et al. 2011). However, the three-dimensional pore space is composed of a variety of different pore types, which vary in size, shape, orientation, and functions (Abou Najm et al. 2010; Katuwal et al. 2015). For example, biopores are voids in the soil that are formed by biological activities such as earthworm burrowing and plant rooting (Kautz 2014). Biopores are usually cylindrical in shape, highly continuous, and can extend along the soil profile (Luo et al. 2010; Wuest 2001). However, non-biopores formed by non-biological activities such as tillage, freezing and thawing or wetting and drying are irregular (packing voids) or sheet-like (cracks) in shape, and extremely variable with water content (Ringrose-Voase 1996; Zhang et al. 2014). Some researchers have demonstrated that the presence of continuous biopores rather than isolated non-biopores significantly increase water infiltration rate, solute transport and air permeability (Bottinelli et al. 2017; Koestel and Larsbo 2014; Naveed et al. 2013). Additionally, biopores provide preferential pathways with low strength for root growth and serve as microbial hotspots of C, N, and P transformations for nutrient acquisition of crop roots (Banfield et al. 2017; Bauke et al. 2017; Han et al. 2015b). The accessibility of macropores by water, plant roots and the release and transport of nutrients is closely related to macropore types and their characteristics; thus, we should differentiate among bulk soil, inter-aggregate, and rhizosphere pore spaces (Pagenkemper et al. 2013).

The difference in morphological features between biopores and non-biopores provides us with the possibility to separate these two types of macropores by image analysis. Previously, two-dimensional images of pore structure were obtained by thin section analysis, and different types of pores such as packing voids, channels, cracks and vughs were distinguished by image analysis (Ringrose-Voase 1996; Ringrose-Voase and Bullock 1984). In recent years, X-ray computed tomography (CT) has been a commonly used tool to explore three-dimensional (3D) soil pore structure noninvasively. Compared with thin sections, CT can identify and visualize small non-connected pores often overlooked by thin sections, and provide more comprehensive

information about 3D pore structure (Alves et al. 2014; Elliot and Heck 2007). The most recent studies investigate 3D soil pore systems integrally or qualitatively describe different types of soil pores using CT (Katuwal et al. 2015; Luo et al. 2008; Zhou et al. 2016). Fewer studies concentrate on direct quantitative characterization of soil biopores vs. non-biopores in 3D. Capowiez et al. (2011) obtained 3D earthworm burrows in artificial soil cores by removing disconnected pore voxel clusters up to a certain size, based on a volume threshold. Pagenkemper et al. (2013) used this method to study characteristics of 3D biopores affected by different cover crops. This method for separating biopores is simple, but does not remove large irregular pores that presumably are not biopores.

In arable soils, biopores in the plough layer are usually destroyed by tillage and their roles may be minimized (Logsdon et al. 1990; Shipitalo et al. 2000; Zhang et al. 2016). However, in the subsoil horizon in which soil is generally supposed to be relatively dense and compacted, biopores are rarely disturbed by tillage and can persist for a long time period (Hagedorn and Bundt 2002; Wuest 2001). For this reason, biopores most likely contribute much to total macroporosity and remarkably influence water and solute transport and root growth in the subsoil (Mossadeghi-Björklund et al. 2016; Nakamoto 2000). Although subsoil is generally less affected by tillage, biopore features in subsoils are presumably influenced by land use and fertilization through crop species with different root morphologies and soil fauna activities (Han et al. 2015a; Köpke et al. 2015). Perkons et al. (2014) found that chicories with a taproot system developed a greater maximum rooting depth and created larger biopores in subsoil than those of the fibrous root system of oats. Inorganic and organic fertilization can increase crop root biomass and change earthworm species, which subsequently alter characteristics of biopores (Marhan and Scheu 2005; Munyankusi et al. 1994; Murchie et al. 2015). However, many studies focus on land use and fertilization effects on 3D macropore structure of topsoil as a whole (Dal Ferro et al. 2012; Zhou et al. 2016), and their effects on the subsoil 3D structure of biopores vs. non-biopores are seldom studied.

Subsoil root exploitation is conducive to greater water and nutrient acquisition for crops (Lynch and Wojciechowski 2015). During root growth, the root apex penetrates the solid soil matrix, and soil particles around roots amalgamate with sloughed cells and

mucilages emitted by both the root and microorganisms surrounding the root (Ghestem et al. 2011). The resulting root channels greatly change the macropore structure of the relatively compacted subsoil, and their features can influence new root elongations (Athmann et al. 2013; Stirzaker et al. 1996). Nevertheless, the 3D characteristics of root channels and other biopores in subsoil are probably variable with land use and fertilization, which require thorough study. In this study, two land uses, paddy field and upland field, were chosen, in which three fertilizations (Control, NPK, NPK plus manure) were considered. Intact subsoil cores were sampled and scanned with industrial X-ray CT. An image analysis was conducted to divide the scanned pores into biopores and non-biopores and to investigate their 3D morphological characteristics. We hypothesized that (1) subsoil biopores constitute a larger proportion of total soil macroporosity; and (2) the characteristics of subsoil biopores vs. non-biopores are significantly influenced by land use and fertilization.

## Materials and methods

### Experimental site

In this study, two different land uses were examined, an upland field and a paddy field. The fields are located at the Jiangxi Institute of Red Soil, Jinxian County, Jiangxi Province, China (116°10'E, 28°21'N), with a subtropical climate and a mean annual temperature and precipitation of 17.7 °C and 1727 mm, respectively. Two long-term fertilization experiments in upland and paddy fields were considered. The upland field long-term fertilization experiments were established in 1986, whereas the paddy field long-term fertilization experiments were initiated in 1981 (Yan et al. 2013).

For the upland field, spring maize–autumn maize was the cropping system. Topsoil (0–20 cm) was tilled with a mouldboard plough by cattle before and after the autumn corn season. Manual hoeing was used to prepare the seedbed. The maize was sowed manually with a spacing of 50 cm × 30 cm. Three fertilization treatments were chosen for this study: (1) no fertilizer as a control (Control); (2) inorganic fertilizers applied at the rates of 60 kg N ha<sup>-1</sup>, 30 kg P<sub>2</sub>O<sub>5</sub> ha<sup>-1</sup>, and 60 kg K<sub>2</sub>O ha<sup>-1</sup> for each corn growing season (NPK); and (3) inorganic fertilizers (same rate as NPK) plus 15 t ha<sup>-1</sup> (fresh weight) organic pig manure (NPKM). The experimental

design used 22.2 m<sup>2</sup> plots and was a randomized complete block with three replicates of each treatment.

In the paddy field, the cropping system was early rice–late rice from April to November and fallow in the winter. The paddy field was flooded, tilled and then puddled to the depth of approximately 17 cm with a small machine before transplanting every season. After puddling, the rice seedlings were manually transplanted with a spacing of 20 cm × 20 cm. The paddy field was subjected to the submerged condition during the rice growth period except for a short dry spell during the rice tillering stage. The site had been cultivated with rice for more than 100 years before the experiment. Similar to the upland field, three fertilization treatments were selected for the paddy field: (1) no fertilization as a control (Control); (2) a combination of inorganic fertilizers (NPK), including 90 kg N ha<sup>-1</sup>, 45 kg P<sub>2</sub>O<sub>5</sub> ha<sup>-1</sup>, and 75 kg K<sub>2</sub>O ha<sup>-1</sup> for each season; and (3) combined organic manure and inorganic fertilizers (NPKM), including the same amount of inorganic fertilizer as the NPK treatment plus 22.5 t ha<sup>-1</sup> (fresh weight) pig manure. The experimental design used 46.7 m<sup>2</sup> plots and was a randomized complete block with three replicates of each treatment.

### Soil sampling and CT scanning

Intact soil cores (5 cm in height and 4.7 cm in diameter) were sampled using PVC cylinders (with downward edge sharpened) from the subsoil (20–30 cm) in the upland field in April 2017 before maize sowing and in the paddy field in November 2016 after rice harvest. We used 6 and 3 replicates for each fertilization treatment in the upland field and paddy field, respectively. Soil cores were wrapped with plastic film and transported to the laboratory for CT scanning. An industrial Phoenix Nanotom X-ray  $\mu$ -CT (GE, Sensing and Inspection Technologies, GmbH, Wunstorf, Germany) was used to scan the soil cores with voltage 110 Kv and current 110  $\mu$ A. A 0.2 mm copper filter was used to alleviate the beam hardening effect. The obtained projections with 1200 images were reconstructed with the software Datos | × 2.0 (GE, Sensing and Inspection Technologies, GmbH, Wunstorf, Germany) using the filtered back-projection algorithm to acquire 8-bit, three-dimensional (2000 × 2000 × 2000 voxels) greyscale images with a voxel resolution of 25  $\mu$ m × 25  $\mu$ m × 25  $\mu$ m. After CT scanning, the soil cores were oven-dried to measure soil bulk density. The disturbed soil samples

were also used to measure soil organic carbon (SOC) with a potassium dichromate oxidation method (Lu 2000) and particle size distribution by laser diffraction particle size analyser (Coulter LS 230; Beckman Coulter, Inc., California, USA). The bulk density, SOC and particle size distribution of the topsoil in each treatment were also measured simultaneously.

### Image analysis and macropore separation

The greyscale images were first filtered with a 3D Gaussian blur filter to reduce noise using the software ImageJ 1.51n. To remove the edge effect caused by sampling, a region of interest (ROI) with the size of  $30 \times 30 \times 25 \text{ mm}^3$  ( $1200 \times 1200 \times 1000$  voxels) was selected from the central part of each soil core. Because of the limitation of data storage and computation capacity of the available computer, the ROI was downscaled by a factor of 2 to obtain a new ROI ( $600 \times 600 \times 500$  voxels, resolution  $50 \text{ }\mu\text{m}$ ) for further image processing and analysis. Segmentation of the greyscale images was performed with 3DMA software (Lindquist and Venkatarangan 1999) using a locally adaptive segmentation method, i.e., the indicator kriging method (Oh and Lindquist 1999). In summary, two cutoff values, one for voids “ $T_0$ ” and the other for solids “ $T_1$ ”, were chosen from the greyscale histogram by visually comparing the segmented image with the original tomogram. The voxels with grey values lower than  $T_0$  and higher than  $T_1$  were classified as voids and solids, respectively. The classification of remaining voxels whose grey values were between  $T_0$  and  $T_1$  was estimated by indicator kriging, which utilizes an estimate of a correlation function incorporating local spatial information (Oh and Lindquist 1999). After segmentation, the pores smaller than 8 voxels, representing  $0.001 \text{ mm}^3$ , were removed to reduce noise.

To separate biopores and non-biopores, the following two assumptions were made: 1) biopores and non-biopores are discrete from one another; 2) biopores are cylindrical and continuous over their length with a certain volume, which are different from the morphological features of non-biopores. For our samples, generally consistent with these two assumptions were the morphological features of biopores and non-biopores. The procedures for separating biopores and non-biopores are presented in Fig. 1. First, the pores smaller than 500 voxels ( $0.06 \text{ mm}^3$ ) were removed (Fig. 1e). The volume threshold was selected in terms of a frequency

distribution of disconnected pore volumes and preservation of cylindrical pores. The selected volume threshold could remove most of disconnected soil pores without cylindrical ones to facilitate the following procedures (Figs. 2 and 1b, e). Second, the ratio of pore length ( $L$ ) to pore equivalent radius ( $r$ ) was defined. The pore length was roughly equal to the diagonal length of bounding box of the pore. The equivalent radius of a pore was equal to:

$$r = \sqrt{\frac{V}{\pi L}} \quad (1)$$

where  $V$  is the volume of the pore. The pores with a ratio ( $L/r$ ) that was less than 20 were considered as non-biopores and removed (Fig. 1f). We chose the ratio threshold value based on several attempts (Fig. 3a, b, c, d, e and f). We plotted the curve between porosities of remaining pores and ratio values and found the ratio value of 20 was approximately at the inflection point (Fig. 3g). Furthermore, the different three-dimensional pore systems that resulted from different ratio values were carefully compared, and finally, the ratio threshold of 20 was considered the most reasonable for distinguishing biopores and non-biopores. For paddy subsoil, the above two steps were effective in obtaining biopores. However, for upland subsoil, a few of the pores obtained after the above two steps did not appear to be biopores based on visual observation, which were removed manually in the third step (Fig. 1g). Then, biopores were acquired (Fig. 1d). Fourth, non-biopores (Fig. 1h) were equal to the difference between total macropores (Fig. 1a) and biopores. These procedures were accomplished with the software MATLAB 2012a (2012).

The separated biopores and non-biopores were analysed to determine porosity, mean pore volume (MPV), total pore surface area (SA), compactness, and connectivity using the software ImageJ 1.51n. Porosity was calculated as the percentage of the pore volume to the total volume of the ROI. The SA is a dimensionless parameter that was calculated as the sum of surface area of all the pores relative to the outer surface area of the ROI (Houston et al. 2017). The compactness of a macropore was defined as:

$$\text{compactness} = \frac{\sqrt[1.5]{A}}{V} \quad (2)$$

where  $A$  is the surface area of the pore. The compactness is dimensionless and minimized by a sphere (Bribiesca

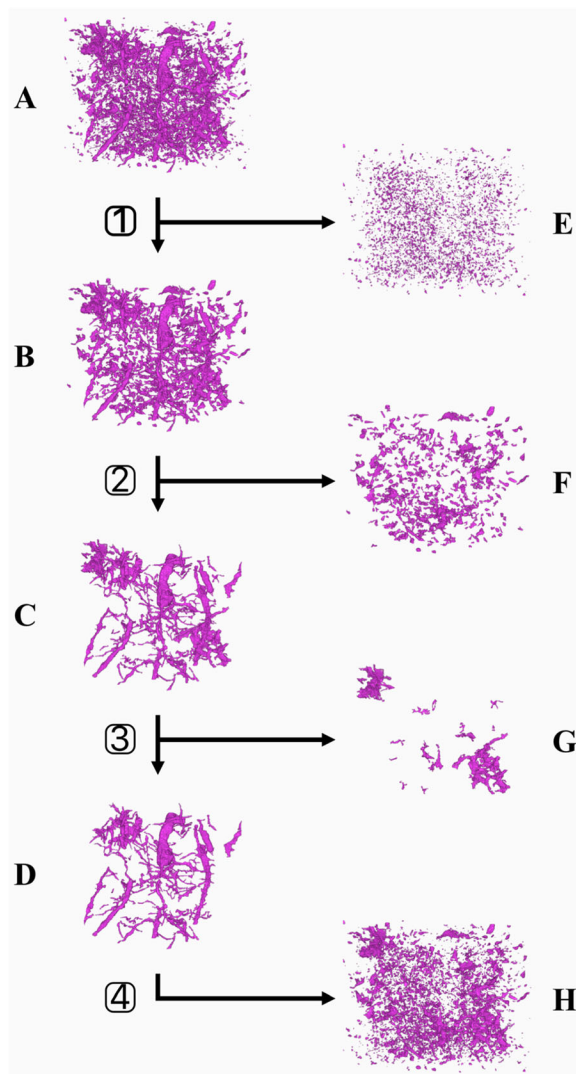


**Fig. 1** The proposed procedure for separating biopores and non-biopores in this study. A is the total macropores after removing noise (<8 voxels); B is the macropores with size larger than 500 voxels; C is the macropores with size larger than 500 voxels and ratio of pore length (L) to pore equivalent radius (r) larger than 20; D is the biopores; E is the macropores with size smaller than 500 voxels (A-B); F is the macropores with size larger than 500 voxels and ratio (L/r) lower than 20 (B-C); G is the macropores manually deleted from the macropores c; H is the non-biopores (A-D). The numbers 1 to 4 in the box indicate four steps for separating biopores and non-biopores

2000). The larger the compactness of a pore, the more the shape deviates from a sphere and the more complex is the structure. The mean compactness (CP) was computed as the volume weighted average of compactness of each pore:

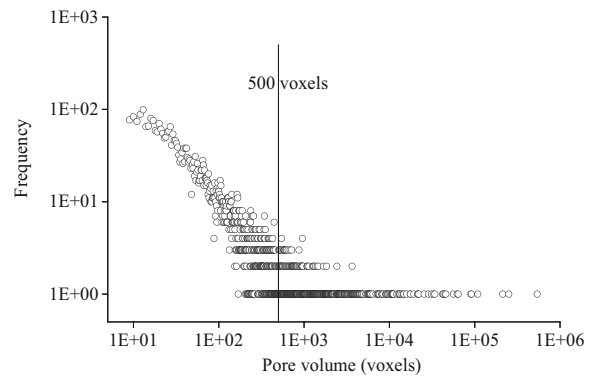


**Fig. 2** Frequency distribution of disconnected pore volumes of one selected soil core and the selected volume threshold

$$CP = \frac{\sum_{i=0}^n CP_i V_i}{\sum_{i=0}^n V_i} \tag{3}$$

where  $i$  is the index of a macropore,  $n$  is the number of macropores, and  $V_i$  is the volume of a macropore. The connectivity was estimated as the volume fraction of pore space that connected with the surface of the ROI volume using the 3D object counter plugin in ImageJ 1.51n (Houston et al. 2013).

Because skeletonization of irregular non-biopores may produce noisy skeletons and cause overestimation of the length (Luo et al. 2010; Peth et al. 2008), only biopores were subjected to skeletonization for measuring length density (LD), tortuosity, branch angle (angle), and mean branch number (MBN). The macropore length was equal to the length of skeletons. Length density was the length of macropores in a unit volume of soil. The tortuosity was calculated as ratio of the total macropore length to the total Euclidean distance (distance between two extreme points of a branch). The inclination of macropore branch was characterized by an angle ( $\theta$ ) between a line that passes two extreme points of the branch and the horizontal plane. The branches with Euclidean distance larger than 1 mm were considered for calculating the angles to reduce the effect of noisy skeletons. The mean angle ( $\theta$ ) was calculated as

$$\theta = \frac{\sum_{i=0}^n L_{ei} \theta_i}{\sum_{i=0}^n L_{ei}} \tag{4}$$

where  $i$  is the index of a macropore branch,  $n$  is the number of branches, and  $L_{ei}$  is the Euclidean distance of a branch. The mean branch number was the total number of branches divided by the number of biopores. The pore size distribution was analysed with a local thickness

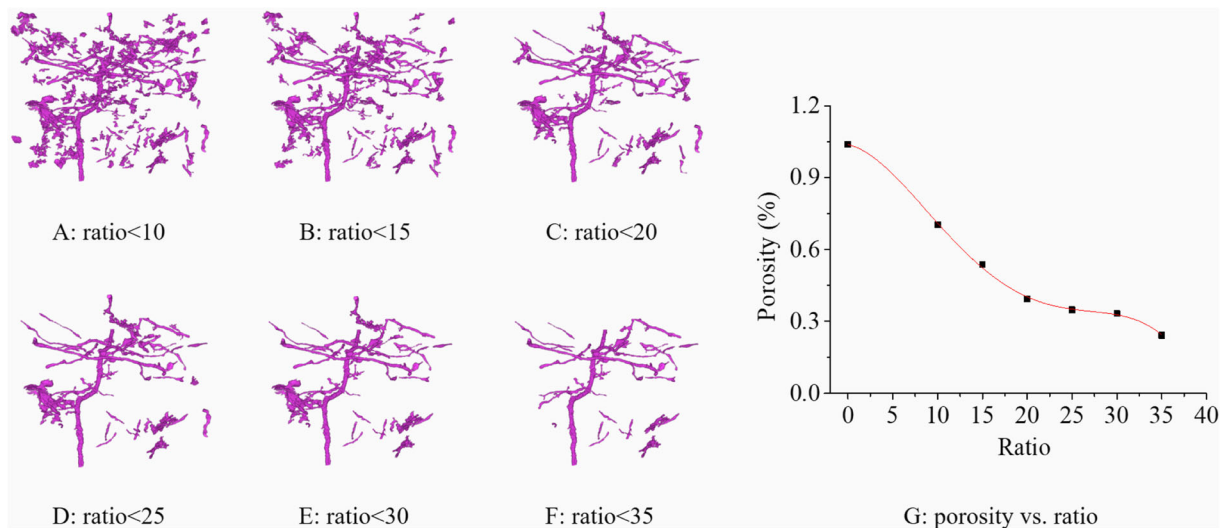


**Fig. 3** Examples of three-dimensional images of soil macropores after removing pores with size smaller than 500 voxels and with ratios of pore length (L) to pore equivalent radius (r) lower than 10

(A), 15(B), 20 (C), 25 (D), 30 (E), and 35 (F), and the relation between porosity of remaining pores and ratio (G)

algorithm, which defines the thickness as the diameter of the greatest sphere that fits within the pore at a specific point (Dougherty and Kunzelmann 2007). After the thickness calculation, the pore system was composed of series of spheres of different diameters, and the pore volumes of different diameters could be counted.

### Statistics

The influence of land use, fertilization or macropore type on 3D characteristics of pore structure was tested by analysis of variance at the significance levels of  $p = 0.05$ ,  $p = 0.01$  and  $p = 0.001$ . The least significant difference (LSD) was used to assess significant differences in 3D characteristics of biopores or non-biopores among the treatments at the  $p = 0.05$  level. The above analyses were performed with the statistical software package IBM SPSS Statistics 19.

## Results

### Soil properties

Compared with the surface layer, the subsoil (20–30 cm) had lower organic carbon, but higher bulk density and clay content (Table 1). For the subsoil, the bulk density was higher in the paddy field than that in the upland field (1.53 vs. 1.45 g cm<sup>-3</sup>), which was in contrast to

bulk density of the topsoil. The clay content increased from 48.5% in the topsoil to 51.3% in the subsoil for the upland field, whereas in the paddy field, clay content increased from 38.8% in the topsoil to 46.3% in the subsoil. The NPKM treatment not only increased SOC in the topsoil but also in the subsoil relative to that in NPK and Control treatments for both land uses.

### Separation of the biopores and non-biopores

As shown in Figs. 4 and 5, the biopores derived from root channels, earthworm burrows, and activities of other soil fauna were generally cylindrical in shape, relatively large, and continuous over their length; whereas the non-biopores were smaller, scattered, more irregular and disconnected. The different morphological features of the separated biopores and non-biopores were consistent with our assumptions, confirming that our methodology was effective in isolating biopores and non-biopores. For the biopores, the thicker or tortuous ones were probably earthworm burrows but difficult to isolate from root channels.

The difference between the biopores and non-biopores was quantitatively analysed. The proportion of biopores to total macroporosity ranged from 30.1 to 74.1% with an average value of 58.5% for all treatments (Fig. 6). The biopores and non-biopores were significantly different in MPV, CP and connectivity, with the exceptions porosity and SA, indicating that the two pore types were

**Table 1** Soil bulk density, soil organic carbon (SOC), and particle size distribution in two land uses and three fertilization treatments

Land use	Soil depth	Fertilization	Bulk density g cm <sup>-3</sup>	SOC g kg <sup>-1</sup>	<2 μm %	2–50 μm	>50 μm
Upland soil	0–20 cm	Control	1.33	13.7	49.3	41.3	9.5
		NPK	1.36	14.6	48.7	41.1	10.3
		NPKM	1.33	20.8	47.7	42.7	9.6
	20–30 cm	Control	1.46	9.76	50.7	41.6	7.7
		NPK	1.45	9.87	51.4	41.8	6.8
		NPKM	1.44	11.5	51.6	41.3	7.1
Paddy soil	0–20 cm	Control	1.26	18.9	38.4	54.5	7.1
		NPK	1.22	18.3	39.8	52.4	7.9
		NPKM	1.11	22.8	38.3	53.5	8.2
	20–30 cm	Control	1.52	15.8	46.2	47.7	6.1
		NPK	1.54	14.0	45.6	48.9	5.4
		NPKM	1.53	17.1	47.0	48.9	4.1

significantly different in morphological features but not in total amount (Table 2). The MPV of the biopores was 55.1-fold larger than that of the non-biopores (Tables 3 and 4). The CP and connectivity of biopores were 3.77 and 8.13-fold greater than those of the non-biopores on average for each treatment, respectively. The diameter of the biopores with the dominant size of 0.25–0.50 mm was generally larger than that of the non-biopores with the dominant size of 0.10–0.25 mm (Fig. 7).

#### Land use effect on characteristics of biopores and non-biopores

The porosities of the total macropores and non-biopores were significantly higher in the upland subsoil than those in the paddy subsoil (Table 2 and Fig. 6). Although land use effect on the biopore porosity was not significant, the proportion of the biopores to total macroporosity was significantly larger in the paddy subsoil than that in the upland subsoil (70.6 vs. 46.3%). For the biopores, the MPV was significantly higher in the upland subsoil than that in the paddy subsoil (Table 3). For the non-biopores, the MPV, SA and connectivity were significantly higher in the upland subsoil than those in the paddy subsoil (Tables 2 and 3). Generally, for those features measured for both the biopores and non-biopores, the land use effect was more evident for the non-biopores than for the biopores. The angle and MBN measured only for the biopores varied significantly between the two land uses. The angle of the biopores was 16.8° higher in the paddy subsoil than that

in the upland subsoil, illustrating that the biopores were more vertically distributed in the paddy subsoil. The upland subsoil had a threefold higher MBN (20.7 vs. 6.9) than that of the paddy subsoil. Additionally, the upland soil had more pore volume with larger diameter than that of the paddy subsoil for both the biopores and non-biopores (Fig. 7). Whereas pore diameters in the paddy subsoil did not exceed 1.0 mm, in the upland subsoil we observed pore diameters up to 4.55 mm.

#### Fertilization effect on characteristics of the biopores and non-biopores

Although in the upland subsoil, the NPK and NPKM treatments showed 2.05 and 2.42-fold higher biopore porosities than that in the Control treatment, the differences were not significant because of the large variation (Fig. 6). The porosity of the non-biopores was very similar among fertilization treatments for each land use. The fertilization treatment did not affect many 3D characteristics of the biopores or non-biopores for both land uses (Tables 3 and 4). However, the tortuosity of the biopores in the NPKM treatment (1.36) was significantly larger than that in the NPK (1.23) and Control (1.23) treatments in the paddy field. Significantly lower in the NPKM treatment than that in the NPK treatment for the paddy subsoil was the angle of the biopores. For the upland subsoil, the NPKM treatment increased the porosity of the biopores with diameters larger than 1.0 mm compared with that in the Control or NPK treatments (Fig. 7).

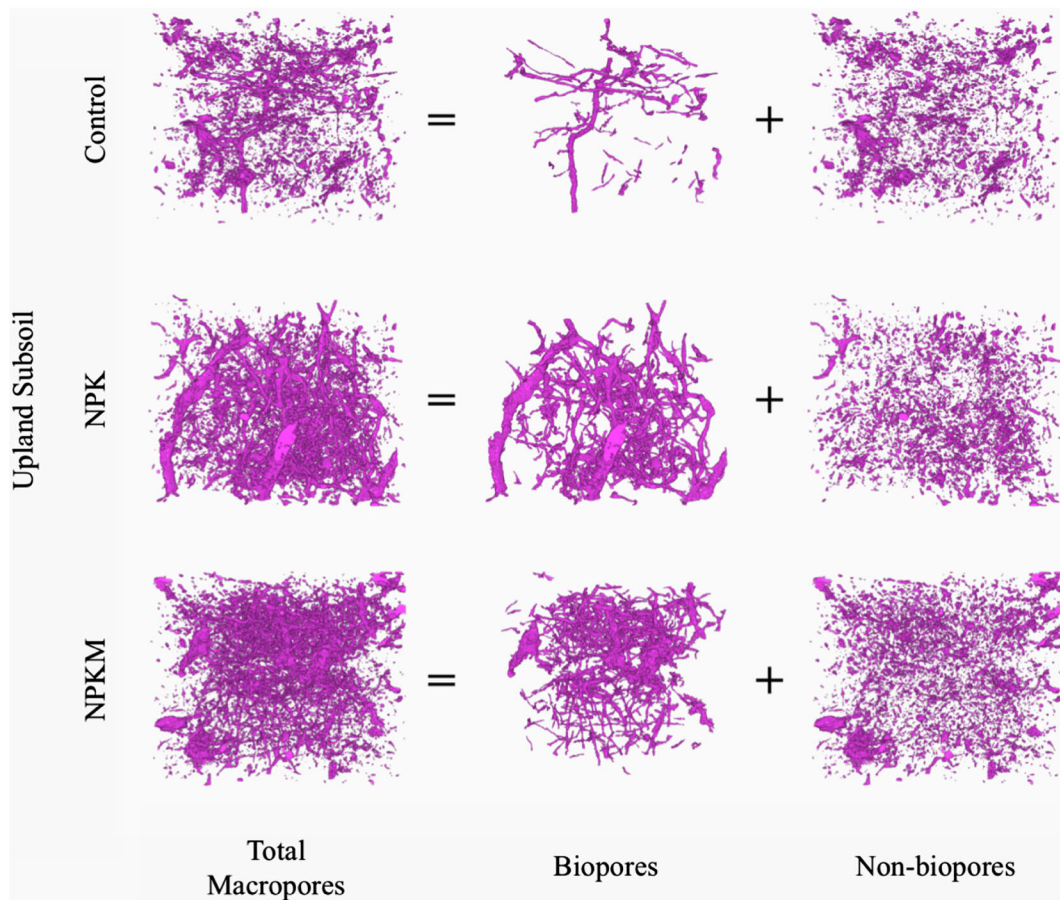


**Fig. 4** Examples of three-dimensional images of soil macropores, biopores and non-biopores of upland subsoil in three different fertilization treatments (The size of 3D soil cores was  $30 \times 30 \times 25$  mm)

## Discussion

In this study, we distinguished the biopores from the non-biopores according to their different 3D morphological characteristics (Fig. 1). In addition to pore volume threshold, a variable ratio of pore length to equivalent radius was also introduced for separating the biopores and non-biopores. To our knowledge, this study is the first to separate the biopores and non-biopores with these two thresholds. In some previous studies, only a volume threshold was used to isolate the biopores from the non-biopores for large soil cores (Bottinelli et al. 2017; Capowiez et al. 2011; Pagenkemper et al. 2013). We found that the subsoil biopores approximately constituted more than half of the total macroporosity. Pagenkemper et al. (2013) found that porosity of biopores ranges from 0.82–1.68%, similar to our observations (0.52–1.55%). In their study, the biopores accounted for 70–80% of total macroporosity, which is slightly higher than our results;

most likely, one reason was that those authors included large, irregular pores into account. Although some old refilled root channels or earthworm burrows were classified as non-biopores in this study, their volumes were small and their functions in conducting water or air were more similar to non-biopores because they were disconnected and less continuous. Compared with the non-biopores, the biopores were generally larger, less compact and more connected based on visualization and quantitative analysis. The biopores with these properties in the subsoil would greatly increase preferential water and nutrient movement downwards (Koestel and Larsbo 2014; Naveed et al. 2016; Sander and Gerke 2007), and consequently reduce water use efficiency and increase potential ground water pollution (Shipitalo et al. 2000; Wopereis et al. 1994). However, these biopores could also facilitate plant root penetration to the subsoil and the uptake of water and nutrients from deeper soil layers (Athmann et al. 2013; Han et al. 2017).



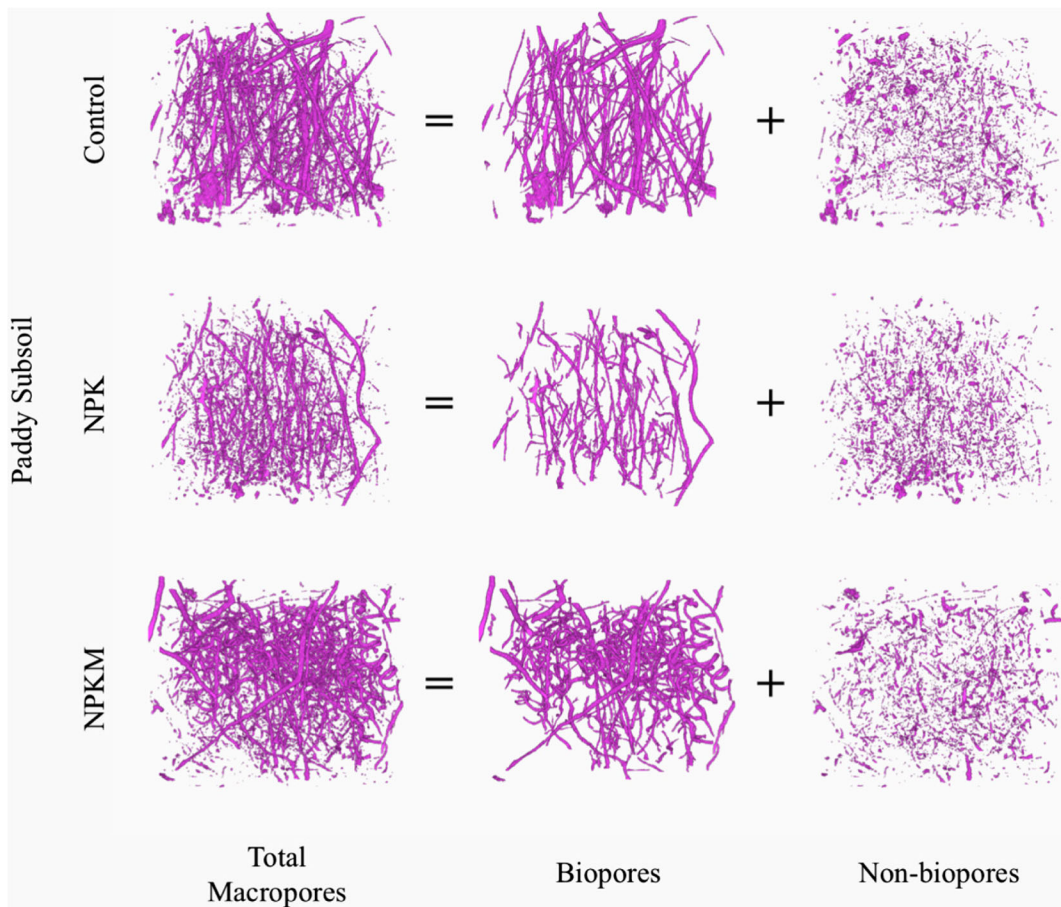


**Fig. 5** Examples of three-dimensional images of soil macropores, biopores and non-biopores of paddy subsoil in three different fertilization treatments (The size of 3D soil cores was 30 × 30 × 25 mm)

**Fig. 6** The porosities of biopores, non-biopores, and total macropores as affected by land use and fertilization. The percentage values indicate the proportion of biopore volume to total macropore volume. Bars are standard errors ( $n = 6$  for upland subsoil and  $n = 3$  for paddy subsoil). Different lowercase and uppercase letters indicate significant difference ( $p < 0.05$ ) in the porosity of biopores and non-biopores among the six treatments, respectively

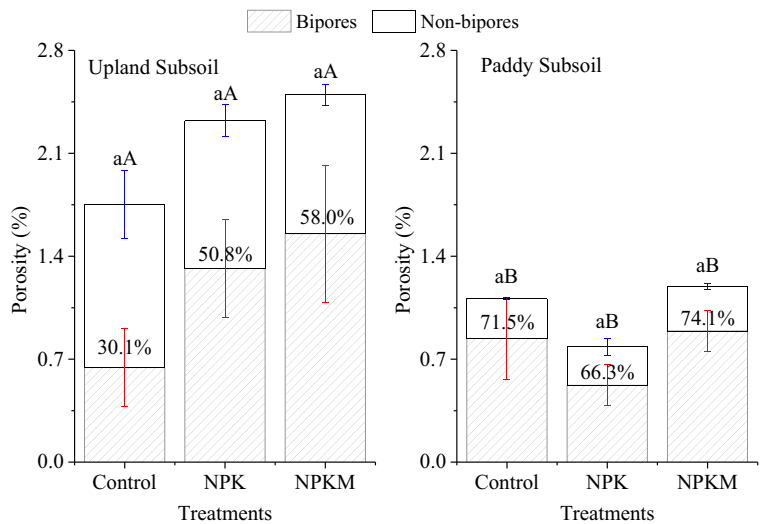


**Table 2** The analysis of variance (ANOVA) on the characteristics of biopores and non-biopores affected by land use and fertilization. The difference between biopores and non-biopores characteristicswas also analyzed with ANOVA. \*, \*\* and \*\*\* represent significant at  $p < 0.5$ , 0.1 and 0.01 level respectively. NS represents not significant

Macropore type	Variation source	Porosity	MPV	SA	CP	Connectivity	PB	LD	Tortuosity	Angle	MBN
Biopore	Land use	NS	**	NS	NS	NS	**	NS	NS	***	**
	Fertilization	NS	NS	NS	NS	NS	NS	NS	**	NS	NS
	Land use * Fertilization	NS	NS	NS	NS	NS	NS	NS	*	NS	NS
Non-biopore	Land use	***	***	***	NS	***					
	Fertilization	NS	NS	NS	NS	NS					
	Land use * Fertilization	NS	NS	NS	NS	NS					
	Macropore type	NS	***	NS	***	***					

MPV mean pore volume, SA surface area, CP compactness, LD length density, PB proportion of biopore volume to total macropore volume, MBN mean branch number

In this study, we found that the 3D characteristics of non-biopores were significantly influenced by land use, because the two land uses were different in tillage and irrigation, which are closely related to formation and destruction of non-biopores. The paddy field is usually subjected to flooding conditions for tillage, puddling, and rice transplanting and growing. The flooding induces soft topsoil with low mechanical strength. As a result, animal hooves or machines easily reach the subsoil during puddling, and a compacted zone (plough pan) with little inter-aggregate pore space is created below the puddled layer, which is intensified by settling and consolidation of dispersed clay particles (Table 1). Moreover, the paddy subsoil is mostly saturated and experiences few wetting and drying (WD) cycles. By

contrast, the upland subsoil is less compacted with lower bulk density and experiences more WD cycles. Therefore, the upland subsoil presented higher MPV, SA and connectivity of non-biopores than those of non-biopores in the paddy subsoil. We discovered that many root channels with diameter ranging from 0.1 to 0.9 mm existed in the paddy subsoil in which the compacted plough pan is located (Fig. 5 and Table 1), indicating that rice roots are able to penetrate the compacted plough pan to create vertical channels (Sander et al. 2008). Furthermore, the porosity of biopores was not significantly different between the paddy subsoil and the upland subsoil, although the former was much denser than the latter (Tables 1 and 2). The results clarified that even in highly compacted paddy subsoil biological activities

**Table 3** Characteristics of biopores derived from CT image analysis in two land uses and three fertilization treatments. The number are presented as mean (standard error,  $n = 6$  for upland soil and  $n = 3$  for paddy soil)

Land use	Fertilization	MPV mm <sup>3</sup>	SA	CP	Connectivity %	LD mm cm <sup>-3</sup>	Tortuosity	Angle	MBN
Upland subsoil (20–30 cm)	Control	1.78(0.51) ab	0.44(0.19) a	176.1(48.4) ab	0.51(0.22) a	64.8(29.9) a	1.26(0.01) b	32.5(4.12) c	15.9(4.4) abc
	NPK	2.87(0.41) a	0.78(0.19) a	340.7(89.7) a	1.10(0.30) a	104.7(26.9) a	1.28(0.00) b	29.6(2.22) c	25.5(5.3) a
	NPKM	2.65(0.46) a	0.81(0.21) a	232.1(64.1) ab	1.25(0.48) a	118.4(33.8) a	1.28(0.01) b	32.3(1.56) c	20.7(3.7) ab
Paddy subsoil	Control	0.89(0.21) b	0.65(0.19) a	140.4(27.2) ab	0.65(0.26) a	100.4(26.4) a	1.23(0.01) b	50.6(1.97) ab	7.4(0.8) bc
	NPK	0.91(0.18) b	0.38(0.07) a	93.9(0.96) b	0.38(0.12) a	51.9(9.59) a	1.23(0.01) b	55.5(2.92) a	5.8(0.5) c
	NPKM	1.17(0.14) b	0.69(0.12) a	148.8(13.2) ab	0.64(0.10) a	99.1(18.2) a	1.36(0.07) a	44.2(2.41) b	7.4(0.6) c

The different lowercase letters indicate significant difference in each column ( $P < 0.05$ )

MPV mean pore volume, SA surface area, CP compactness, LD length density, MBN mean branch number

**Table 4** Characteristics of non-biopores derived from CT image analysis in two land uses and three fertilization treatments.

Land use	Fertilization	MPV mm <sup>3</sup>	SA	CP	Connectivity %
Upland subsoil	Control	0.050(0.01) a	1.13(0.21) a	81.3(15.7) a	0.31(0.08) a
	NPK	0.041(0.00) a	1.05(0.10) a	51.3(4.27) ab	0.21(0.03) a
	NPKM	0.037(0.00) ab	1.01(0.08) a	53.1(4.10) ab	0.24(0.01) a
Paddy subsoil	Control	0.018(0.00) b	0.36(0.01) b	35.4(1.45) b	0.052(0.01) b
	NPK	0.021(0.01) b	0.34(0.06) b	71.5(37.6) ab	0.035(0.01) b
	NPKM	0.020(0.00) b	0.41(0.03) b	36.0(0.75) b	0.049(0.01) b

The numbers are presented as mean (standard error, n = 6 for upland soil and n = 3 for paddy soil). The different lowercase letters indicate significant difference in each column (*p* < 0.05)

MPV mean pore volume, SA surface area, CP compactness

such as rice rooting were abundant, similar to those in the upland subsoil. Thus, the proportion of biopore volume to total macropore volume was significantly higher in the paddy subsoil than that in the upland subsoil (Table 2). The biopores in the paddy subsoil were thinner and more vertically distributed with fewer branches than those in the upland subsoil (Table 3), which could be attributed to different root morphologies and activities of soil fauna between the two land uses. Yamauchi et al. (1987) reported that rice

has more nodal roots with a relatively small rooting angle that develop towards the direction immediately below the rice shoots, whereas maize develops fewer but longer nodal roots of which most run obliquely in the soil with a relatively larger rooting diameter than roots of rice. The difference in root morphology between rice and maize revealed by Yamauchi et al. (1987) is consistent with the difference in characteristics of root channels between the paddy field and the upland field in this study, where rice and maize were

**Fig. 7** The pore size distribution of biopores and non-biopores as affected by land use and fertilization. Bars are standard errors (n = 6 for upland subsoil and n = 3 for paddy subsoil)

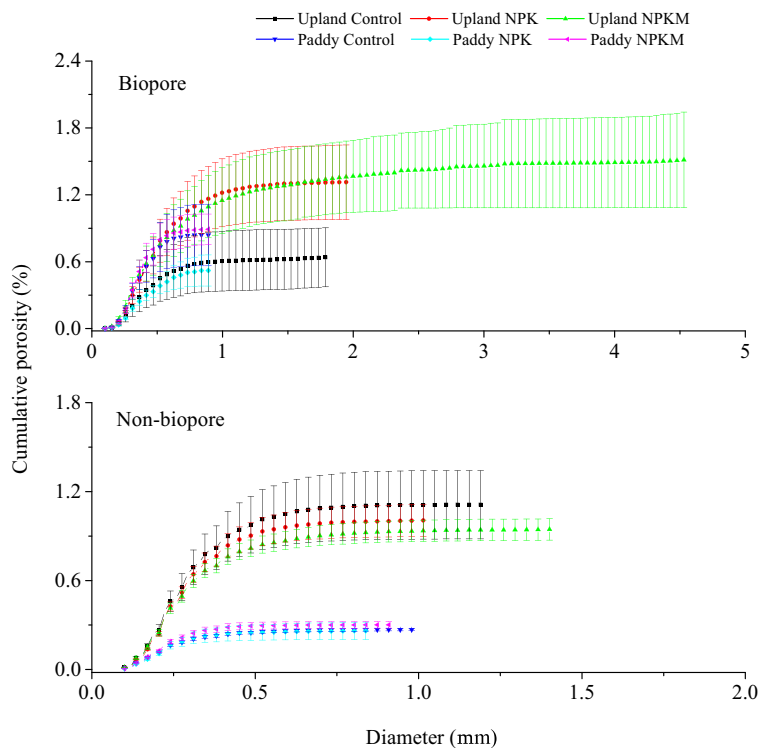
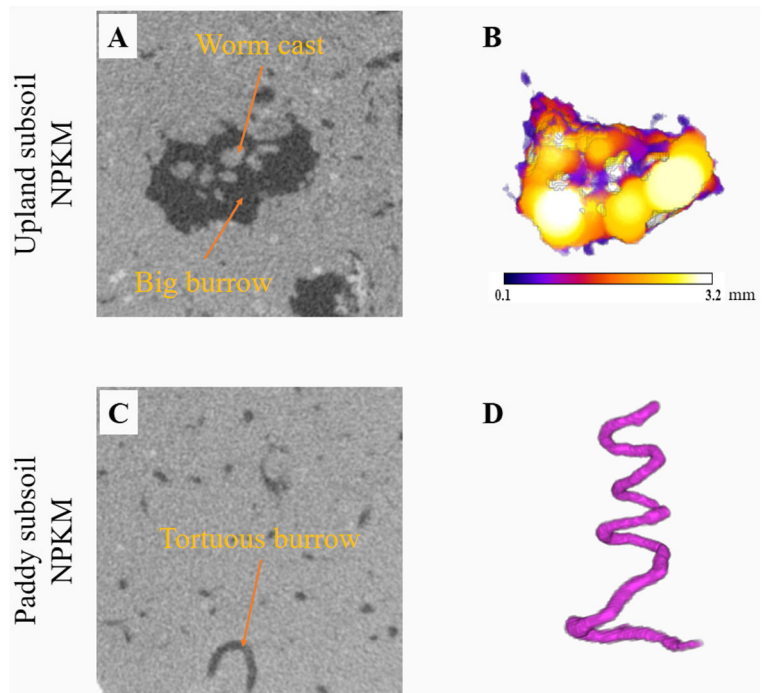


**Fig. 8** Examples of large or tortuous burrows in 2D and 3D in manure applied treatments in the two land uses. **a** One 2D large burrow in NPKM treatment in upland subsoil (image size 15×15 mm); **b** 3D thickness map of the large burrow in NPKM treatment in upland subsoil (object bounding box size 10.25×8.95×5.15 mm; the different colors indicate different thicknesses); **c** One 2D tortuous burrow in NPKM treatment in paddy subsoil (image size 15×15 mm); **d** 3D image of the tortuous burrow in NPKM treatment in paddy subsoil (object bounding box size 4.15×4.55×8.00 mm)



continuously planted, respectively. The results indicate that root morphology of different crop species prominently shapes subsoil biopore features. The activities of soil fauna in paddy fields are considered to be less frequent than those in upland fields due to the long time under submerged conditions (Plum and Filser 2005; Zorn et al. 2008). Thus, soil fauna burrows with large diameter were only observed for the upland subsoil from the CT images (Fig. 8).

In some studies, organic fertilization changes 3D pore structure of topsoil compared with that of non-fertilization (Zhou et al. 2016; Zhou et al. 2013). Few studies have examined the fertilization effect on 3D pore structure of subsoil with CT scanning where tillage is usually absent. Schlüter et al. (2011) found that fertilization does not change 3D pore connectivity and pore size distribution of the subsoil. In this study, fertilization treatments had little influence on 3D non-biopore features of subsoil (Table 4). Physical forces such as wetting-drying cycles and tillage, are most responsible for forming non-biopores. Moreover, these physical forces were almost identical among the three fertilization treatments in each land use, particularly for the subsoil. However, the biopores formed by biological forces were higher in tortuosity and lower in angle in the manure-applied treatment than in the two other treatments for the

paddy subsoil (Table 3 and Fig. 8c, d). Additionally, manure application also increased biopore volume with large diameters for the upland subsoil (Figs. 7 and 8a, b). These results can be explained by the fact that manure application generally increases SOC in the subsoil (Table 1), and consequently increases biomass or changes species of soil fauna (Marhan and Scheu 2005; Munyankusi et al. 1994; Murchie et al. 2015). Earthworm burrow features in the soil depend on both the earthworm abundance and the local composition of the earthworm community (Bastardie et al. 2005; Bottinelli et al. 2017). Munyankusi et al. (1994) discovered that a deep burrowing species *L. terrestris*, which can form channels with diameter up to 10 mm and extend to more than 1 m in depth, was in manure-applied plots rather than in inorganic fertilizer plots in continuous maize planted soil.

## Conclusions

The influences of land use and fertilization on the 3D characteristics of subsoil biopores and non-biopores were studied using CT and image analysis. According to different 3D morphological characteristics, the biopores and non-biopores were well separated by

introducing a variable ratio of pore length to equivalent radius. The proportion of biopore volume to the total macropore volume was more than half on average, which was significantly influenced by land use. The land use effect on porosity, MPV, SA and connectivity of non-biopores was significant. Unlike the non-biopores, the MPV, angle and MBN of the biopores were significantly influenced by land use. Fertilization had a minor effect on the non-biopore characteristics, but manure application increased the biopore volume with large diameters for the upland subsoil, and changed the tortuosity and the angle of the biopores for the paddy subsoil. Our results reveal that the responses of the subsoil biopore and non-biopore characteristics to land use and fertilization are different.

We found that the biopores were much more continuous than the non-biopores. Thus, the inference is that biopore characteristics would be more effective in predicting water flow and solute transport than those of non-biopores or total macropores, which requires verification in future studies. Furthermore, this study implies that subsoil biopore characteristics are a function of crop species and fertilization strategies, which indicates that different crop species and fertilization strategies can modify subsoil pore structure. This outcome provides us with a new perspective that subsoil constraints such as compaction, which are difficult to remove by conventional tillage, could be ameliorated by reasonable arrangement of crop rotation and manure application.

**Acknowledgements** This National Natural Science Foundation of China (NSFC 41401245, 41771264 and 41571130053), Innovation Program of the Institute of Soil Science CAS, China (No. ISSASIP1610) and State Key Laboratory of Soil and Sustainable Agriculture (Y20160012) provided financial support for this study. Xinhua Peng is grateful to the National Science Foundation for Distinguished Young Scholars (41725004). The authors thank the staff at Jiangxi Institute of Red Soil who conducted and maintained the two long-term field experiments.

## References

- Abou Najm MR, Jabro JD, Iversen WM, Mohtar RH, Evans RG (2010) New method for the characterization of three-dimensional preferential flow paths in the field. *Water Resour Res* 46:W02503. <https://doi.org/10.1029/2009wr008594>
- Alves H, Lima I, Assis JT, Geraldes M, Lopes RT (2014) Comparison of pore space features by thin sections and X-ray microtomography. *Appl Radiat Isot* 94:182–190. <https://doi.org/10.1016/j.apradiso.2014.08.003>
- Athmann M, Kautz T, Pude R, Köpke U (2013) Root growth in biopores—evaluation with in situ endoscopy. *Plant Soil* 371:179–190. <https://doi.org/10.1007/s11104-013-1673-5>
- Banfield CC, Dippold MA, Pausch J, Hoang DTT, Kuzyakov Y (2017) Biopore history determines the microbial community composition in subsoil hotspots. *Biol Fertil Soils* 53:573–588. <https://doi.org/10.1007/s00374-017-1201-5>
- Bastardie F, Capowiez Y, Cluzeau D (2005) 3D characterisation of earthworm burrow systems in natural soil cores collected from a 12-year-old pasture. *Appl Soil Ecol* 30:34–46
- Bauke SL, von Sperber C, Siebers N, Tamburini F, Amelung W (2017) Biopore effects on phosphorus biogeochemistry in subsoils. *Soil Biol Biochem* 111:157–165. <https://doi.org/10.1016/j.soilbio.2017.04.012>
- Bottinelli N, Zhou H, Capowiez Y, Zhang ZB, Qiu J, Jouquet P, Peng XH (2017) Earthworm burrowing activity of two non-Lumbricidae earthworm species incubated in soils with contrasting organic carbon content (vertisol vs. Ultisol). *Biol Fertil Soils* 53:951–955. <https://doi.org/10.1007/s00374-017-1235-8>
- Bribiesca E (2000) A measure of compactness for 3D shapes. *Computers & Mathematics with Applications* 40:1275–1284. [https://doi.org/10.1016/S0898-1221\(00\)00238-8](https://doi.org/10.1016/S0898-1221(00)00238-8)
- Capowiez Y, Sammartino S, Michel E (2011) Using X-ray tomography to quantify earthworm bioturbation non-destructively in repacked soil cores. *Geoderma* 162:124–131
- Dal Ferro N, Delmas P, Duwig C, Simonetti G, Morari F (2012) Coupling X-ray microtomography and mercury intrusion porosimetry to quantify aggregate structures of a cambisol under different fertilisation treatments. *Soil Tillage Res* 119:13–21. <https://doi.org/10.1016/j.still.2011.12.001>
- Dougherty R, Kunzelmann KH (2007) Computing local thickness of 3D structures with image J. *Microsc Microanal* 13:1678–1679
- Elliot TR, Heck RJ (2007) A comparison of optical and X-ray CT technique for void analysis in soil thin section. *Geoderma* 141:60–70. <https://doi.org/10.1016/j.geoderma.2007.05.001>
- Ghestem M, Sidle RC, Stokes A (2011) The influence of plant root systems on subsurface flow: implications for slope stability. *Bio Science* 61:869–879. <https://doi.org/10.1525/bio.2011.61.11.6>
- Hagedorn F, Bundt M (2002) The age of preferential flow paths. *Geoderma* 108:119–132. [https://doi.org/10.1016/S0016-7061\(02\)00129-5](https://doi.org/10.1016/S0016-7061(02)00129-5)
- Han E, Kautz T, Perkons U, Lüsebrink M, Pude R, Köpke U (2015a) Quantification of soil biopore density after perennial fodder cropping. *Plant Soil*:1–13. <https://doi.org/10.1007/s11104-015-2488-3>
- Han E, Kautz T, Perkons U, Uteau D, Peth S, Huang N, Horn R, Köpke U (2015b) Root growth dynamics inside and outside of soil biopores as affected by crop sequence determined with the profile wall method. *Biol Fertil Soils*:1–10. <https://doi.org/10.1007/s00374-015-1032-1>
- Han E, Kautz T, Huang N, Köpke U (2017) Dynamics of plant nutrient uptake as affected by biopore-associated root growth in arable subsoil. *Plant Soil* 415:145–160. <https://doi.org/10.1007/s11104-016-3150-4>
- Houston AN, Schmidt S, Tarquis AM, Otten W, Baveye PC, Hapca SM (2013) Effect of scanning and image

- reconstruction settings in X-ray computed microtomography on quality and segmentation of 3D soil images. *Geoderma* 207–208:154–165. <https://doi.org/10.1016/j.geoderma.2013.05.017>
- Houston AN, Otten W, Falconer R, Monga O, Baveye PC, Hapca SM (2017) Quantification of the pore size distribution of soils: assessment of existing software using tomographic and synthetic 3D images. *Geoderma* 299:73–82. <https://doi.org/10.1016/j.geoderma.2017.03.025>
- Katuwal S, Norgaard T, Moldrup P, Lamandé M, Wildenschild D, de Jonge LW (2015) Linking air and water transport in intact soils to macropore characteristics inferred from X-ray computed tomography. *Geoderma* 237:9–20. <https://doi.org/10.1016/j.geoderma.2014.08.006>
- Kautz T (2014) Research on subsoil biopores and their functions in organically managed soils: a review. *Renewable Agriculture and Food Systems* 30:318–327
- Koestel J, Larsbo M (2014) Imaging and quantification of preferential solute transport in soil macropores. *Water Resour Res* 50:4357–4378
- Köpke U, Athmann M, Han E, Kautz T (2015) Optimising cropping techniques for nutrient and environmental management in organic agriculture. *Sustainable Agriculture Research* 4:15–25
- Lamandé M, Labouriau R, Holmstrup M, Torp SB, Greve MH, Heckrath G, Iversen BV, de Jonge LW, Moldrup P, Jacobsen OH (2011) Density of macropores as related to soil and earthworm community parameters in cultivated grasslands. *Geoderma* 162:319–326. <https://doi.org/10.1016/j.geoderma.2011.03.004>
- Lindquist WB, Venkatarangan A (1999) Investigating 3D geometry of porous media from high resolution images. *Phys Chem Earth Solid Earth Geod* 24:593–599
- Logsdon SD, Allmaras RR, Wu L, Swan JB, Randall GW (1990) Macroporosity and its relation to saturated hydraulic conductivity under different tillage practices. *Soil Sci Soc Am J* 54:1096–1101. <https://doi.org/10.2136/sssaj1990.03615995005400040029x>
- Lu R (2000) *Methods of soil and agricultural chemistry analysis (in Chinese)*. China Agricultural Science and Technology Press
- Luo L, Lin H, Halleck P (2008) Quantifying soil structure and preferential flow in intact soil using X-ray computed tomography. *Soil Sci Soc Am J* 72:1058–1069
- Luo L, Lin H, Li S (2010) Quantification of 3-D soil macropore networks in different soil types and land uses using computed tomography. *J Hydrol* 393:53–64
- Lynch JP, Wojciechowski T (2015) Opportunities and challenges in the subsoil: pathways to deeper rooted crops. *Journal of Experimental Botany*:eru508
- Marhan S, Scheu S (2005) The influence of mineral and organic fertilisers on the growth of the endogeic earthworm *Octolasion tyraeum* (Savigny). *Pedobiologia* 49:239–249. <https://doi.org/10.1016/j.pedobi.2004.11.002>
- MATLAB 2012a (2012) The MathWorks, Inc., Natick, Massachusetts, United States
- Mossadeghi-Björklund M, Arvidsson J, Keller T, Koestel J, Lamandé M, Larsbo M, Jarvis N (2016) Effects of subsoil compaction on hydraulic properties and preferential flow in a Swedish clay soil. *Soil Tillage Res* 156:91–98. <https://doi.org/10.1016/j.still.2015.09.013>
- Munyankusi E, Gupta SC, Moncrief JF, Berry EC (1994) Earthworm macropores and preferential transport in a long-term manure applied Typic Hapludalf. *J Environ Qual* 23:773–784. <https://doi.org/10.2134/jeq1994.00472425002300040023x>
- Murchie AK, Blackshaw RP, Gordon AW, Christie P (2015) Responses of earthworm species to long-term applications of slurry. *Appl Soil Ecol* 96:60–67. <https://doi.org/10.1016/j.apsoil.2015.07.005>
- Nakamoto T (2000) The distribution of wheat and maize roots as influenced by biopores in a subsoil of the Kanto loam type. *Plant Production Science* 3:140–144
- Naveed M, Moldrup P, Arthur E, Wildenschild D, Eden M, Lamandé M, Vogel HJ, de Jonge LW (2013) Revealing soil structure and functional macroporosity along a clay gradient using X-ray computed tomography. *Soil Sci Soc Am J* 77:403–411
- Naveed M, Moldrup P, Schaap MG, Tuller M, Kulkarni R, Vogel HJ, Jonge LWD (2016) Prediction of biopore- and matrix-dominated flow from X-ray CT-derived macropore network characteristics. *Hydrol Earth Syst Sci Discuss* 20:4017–4030
- Oh W, Lindquist WB (1999) Image thresholding by indicator kriging. *IEEE Trans Pattern Anal Mach Intell* 21:590–602
- Pagenkemper SK, Peth S, Puschmann DU, Horn R (2013) Effects of root-induced biopores on pore space architecture investigated with industrial X-ray computed tomography. In: Anderson SH, Hopmans JW (eds) *Soil–water–root processes: advances in tomography and imaging*. SSSA special publication. The soil science Society of America, Inc, pp 69–96. <https://doi.org/10.2136/sssaspecpub61.c4>
- Perkons U, Kautz T, Uteau D, Peth S, Geier V, Thomas K, Lütke Holz K, Athmann M, Pude R, Köpke U (2014) Root-length densities of various annual crops following crops with contrasting root systems. *Soil Tillage Res* 137:50–57. <https://doi.org/10.1016/j.still.2013.11.005>
- Peth S, Horn R, Beckmann F, Donath T, Fischer J, Smucker AJM (2008) Three-dimensional quantification of intra-aggregate pore-space features using synchrotron-radiation-based microtomography. *Soil Sci Soc Am J* 72:897–907. <https://doi.org/10.2136/sssaj2007.0130>
- Plum NM, Filser J (2005) Floods and drought: response of earthworms and potworms (Oligochaeta: Lumbricidae, Enchytraeidae) to hydrological extremes in wet grassland. *Pedobiologia* 49:443–453. <https://doi.org/10.1016/j.pedobi.2005.05.004>
- Ringrose-Voase AJ (1996) Measurement of soil macropore geometry by image analysis of sections through impregnated soil. *Plant Soil* 183:27–47. <https://doi.org/10.1007/bf02185563>
- Ringrose-Voase AJ, Bullock P (1984) The automatic recognition and measurement of soil pore types by image analysis and computer programs. *J Soil Sci* 35:673–684. <https://doi.org/10.1111/j.1365-2389.1984.tb00624.x>
- Sander T, Gerke HH (2007) Preferential flow patterns in paddy fields using a dye tracer. *Vadose Zone J* 6:105–115. <https://doi.org/10.2136/Vzj2006.0035>
- Sander T, Gerke HH, Rogasik H (2008) Assessment of Chinese paddy-soil structure using X-ray computed tomography. *Geoderma* 145:303–314
- Schlüter S, Weller U, Vogel H-J (2011) Soil-structure development including seasonal dynamics in a long-term fertilization

- experiment. *J Plant Nutr Soil Sci* 174:395–403. <https://doi.org/10.1002/jpln.201000103>
- Shipitalo MJ, Dick WA, Edwards WM (2000) Conservation tillage and macropore factors that affect water movement and the fate of chemicals. *Soil Tillage Res* 53:167–183. [https://doi.org/10.1016/S0167-1987\(99\)00104-X](https://doi.org/10.1016/S0167-1987(99)00104-X)
- Stirzaker RJ, Passioura JB, Wilms Y (1996) Soil structure and plant growth: impact of bulk density and biopores. *Plant Soil* 185:151–162
- Wopereis M, Bouma J, Kropff M, Sanidad W (1994) Reducing bypass flow through a dry, cracked and previously puddled rice soil. *Soil Tillage Res* 29:1–11
- Wuest SB (2001) Soil biopore estimation: effects of tillage, nitrogen, and photographic resolution. *Soil Tillage Res* 62:111–116. [https://doi.org/10.1016/S0167-1987\(01\)00218-5](https://doi.org/10.1016/S0167-1987(01)00218-5)
- Yamauchi A, Kono Y, Tatsumi J (1987) Quantitative analysis on root system structures of upland rice and maize. *Japanese Journal of Crop Science* 56:608–617
- Yan X, Zhou H, Zhu QH, Wang XF, Zhang YZ, Yu XC, Peng X (2013) Carbon sequestration efficiency in paddy soil and upland soil under long-term fertilization in southern China. *Soil Tillage Res* 130:42–51. <https://doi.org/10.1016/j.still.2013.01.013>
- Zhang ZB, Zhou H, Zhao QG, Lin H, Peng X (2014) Characteristics of cracks in two paddy soils and their impacts on preferential flow. *Geoderma* 228–229:114–121. <https://doi.org/10.1016/j.geoderma.2013.07.026>
- Zhang Z, Lin L, Wang Y, Peng X (2016) Temporal change in soil macropores measured using tension infiltrometer under different land uses and slope positions in subtropical China. *J Soils Sediments* 16:854–863. <https://doi.org/10.1007/s11368-015-1295-z>
- Zhou H, Peng X, Perfect E, Xiao T, Peng G (2013) Effects of organic and inorganic fertilization on soil aggregation in an Ultisol as characterized by synchrotron based X-ray micro-computed tomography. *Geoderma* 195–196:23–30. <https://doi.org/10.1016/j.geoderma.2012.11.003>
- Zhou H, Fang H, Mooney SJ, Peng X (2016) Effects of long-term inorganic and organic fertilizations on the soil micro and macro structures of rice paddies. *Geoderma* 266:66–74
- Zorn MI, Van Gestel CAM, Morrien E, Wagenaar M, Eijsackers H (2008) Flooding responses of three earthworm species, *Allolobophora chlorotica*, *Aporrectodea caliginosa* and *Lumbricus rubellus*, in a laboratory-controlled environment. *Soil Biol Biochem* 40:587–593 <https://doi.org/10.1016/j.soilbio.2007.06.028>